LITHOS 464–465 (2024) 107411

Contents lists available at ScienceDirect

LITHOS

journal homepage: www.elsevier.com/locate/lithos

High-field-strength-element enriched arc rocks witness subducted mélange recycling in upwelling asthenosphere

Huichuan Liu [a,*], Alan R. Hastie [b,*], Chiara Maria Petrone [c]

[a] State Key Laboratory of Petroleum Resources and Prospecting, China University of Petroleum (Beijing), Beijing 102249, China
[b] School of Geosciences, University of Edinburgh, Grant Institute, The King's Buildings, James Hutton Road, Edinburgh EH9 3FE, UK
[c] Volcano Petrology Group, Natural History Museum, London SW7 5BD, UK

ARTICLE INFO

Keywords:
Mélange diapir
Altered oceanic crust
Nb-enriched basalt
Crust-mantle interaction
Oceanic crust recycling

ABSTRACT

Arc rocks, as the most common product of plate subduction factory, are generally characterized by high field strength element (HFSE) depletions. However, HFSE-enriched arc rocks are also identified, and their origin is still controversial. We conduct combined radiogenic and stable isotope analyses on two ocean island basalt (OIB)-associated HFSE-enriched mafic intrusions in the Yunnan-Burma region. Median incompatible trace element compositions argue for a binary mixing between OIB-like asthenosphere dominated mantle source and a complex arc-like component. The high radiogenic Pb [($^{206}Pb/^{204}Pb)i$ = 17.99–18.85, ($^{207}Pb/^{204}Pb)i$ = 15.53–15.71 and ($^{208}Pb/^{204}Pb)i$ = 38.16–39.20] and heavy Mg ($\delta^{26}Mg$ = −0.115‰ to 0.357‰) isotopes could only be inherited from subducted marine sediments. Altered oceanic crust (often abbreviated to AOC) is also involved in the source as evidenced by light Li isotopes ($\delta^{7}Li$ = −2.54‰ to −1.31‰). Therefore, we argue that this arc-like component is inherited from subducted mélange (i.e., bulk marine sediment and AOC) recycling, rather than the more common melt and/or fluid metasomatism. In summary, the OIB associated HFSEs-enriched arc rocks are products of and witnessed the subducted mélange recycling and its interaction with the upwelling asthenosphere.

1. Introduction

The behaviors of high field strength elements (HFSE) during oceanic plate subduction are of great importance to earth sciences because subducted materials modify the Earth's mantle compositions and heavily influence the source regions of mafic lavas (Castillo et al., 2002; Munker et al., 2004). Subduction-derived arc magmas are featured by relative depletions in HFSEs on normalized multielement diagrams when compared with other mantle-derived magmas, i.e., strong HFSE negative anomalies compared with adjacent large ion lithophile elements (LILE) (Kelemen et al., 1990; Munker et al., 2004). However, subordinate HFSE-enriched mafic arc rocks have been found in several modern arcs, such as, the Panama-Costa Rica (Reagan and Gill, 1989), the Trans-Mexican Volcanic Belt (Petrone et al., 2003; Petrone and Ferrari, 2008), the Greater Antilles (Hastie et al., 2007; Hastie et al., 2011) the Cascades (Defant and Drummond, 1993), Kamchatka (Kepezhinskas et al., 1996), Baja California (Aguillon-Robles et al., 2001; Castillo, 2008), and Sulu (Castillo et al., 2002; Castillo et al., 2007). These HFSE-enriched rocks, with much high Nb concentrations (>20 ppm versus <4 ppm for normal arc lavas), have been termed as high-Nb mafic rocks (HNB) (Reagan and Gill, 1989). Mafic rocks with lower absolute Nb concentrations (7–16 ppm) but similar trace element ratios to high-Nb mafic rocks, such as the basalts reported by Sajona et al. (1993) in the Sulu Arc, southern Philippines, are termed as Nb-enriched basalts (NEB).

Normal arc rocks are considered to be originated from the mantle wedge that has been metasomatized by HFSE-poor subducted slab-derived fluids and/or melts, or mélange partial melting (Hall and Kincaid, 2001; Kelemen et al., 1990). Nevertheless, the petrogenesis of Nb-enriched mafic rocks is still controversial. Almost all previous studies argue that Nb-enriched mafic rocks are derived from partial melting of adakitic melt metasomatized mantle (Aguillon-Robles et al., 2001; Azizi et al., 2014; Wang et al., 2008; Wyman et al., 2000). This geochemical model is supported by the fact that adakites and Nb-enriched mafic rocks are erupted more or less simultaneously (Prouteau et al., 2000). However, (1) due to the high Sr/Y and $(La/Yb)_{PM}$ ratios of adakites (Castillo, 2012), their metasomatized mantle wedge should also show high Sr/Y and $(La/Yb)_{PM}$ ratios, in contrast to the extremely low Sr/Y and $(La/Yb)_{PM}$ ratios of the Nb-enriched mafic rocks (Castillo, 2008); (2) both adakite and metasomatized mantle wedge exhibit measurably Nb—Ta negative anomalies in their trace element spider diagrams (Wang et al.,

* Corresponding authors.
E-mail address: liuhuichuan1986@126.com (H. Liu).

https://doi.org/10.1016/j.lithos.2023.107411
Received 13 June 2023; Received in revised form 22 October 2023; Accepted 27 October 2023
Available online 7 November 2023

2008); (3) some Nb-enriched mafic rocks have alkaline or transitional geochemical compositions (Petrone et al., 2003; Petrone and Ferrari, 2008; Righter and Rosas-Elguera, 2001; Verma and Nelson, 1989), and cannot be produced by the metasomatism of the mantle by calc-alkaline adakites. Thus, an alternative explanation for the formation of Nb-enriched mafic rocks is from the partial melting of mixtures between enriched OIB-like and depleted-MORB-like or arc-like mantle (Castillo, 2008; Liu et al., 2017a; Petrone et al., 2003; Petrone and Ferrari, 2008). The frequent association of adakite-Nb-enriched mafic rocks with porphyry Cu—Au mineralization which is believed to be genetic rather than casual (Deng et al., 2020; Kepezhinskas et al., 2022), makes even more compelling to understand which mechanism dominated the petrogenesis of Nb-enriched mafic rocks.

Previous studies have identified four separate suites of Nb-enriched mafic rocks in the Ailaoshan area of the Yunnan-Burma region (Fig. 1b, Supplementary Figs. S1 and S2). Our study sampled and analyzed the Cretaceous Nb-enriched mafic rocks from Mili village (139 Ma; Xinping county) and Yaoshan village (73–68 Ma; Pingbian county) in the Ailaoshan area of the Yunnan-Burma region (Fig. 1). Zircon U—Pb ages, elemental analyses, and Sr—Nd isotopes have been reported in (Liu et al., 2017a). These data, together with Pb-Li-Mg isotope data in this study, enable us to reevaluate the origins of the Nb-enriched arc rocks.

2. Geological background

Southeast Asia is made up of several structural terranes that were assembled during the Neoproterozoic to Phanerozoic (Fig. 1a). In detail this includes (1) Neoproterozoic amalgamation between the South China Craton and the Indochina block, (2) early Paleozoic rifting of South China from Gondwana, (3) latest Permian to Early Triassic Paleotethyan Ocean closure, (4) latest Permian eruption of the Emeishan large igneous province, and (5) Cretaceous-Neogene Neotethyan Ocean closure (Liu et al., 2017a). The NW-trending Ailaoshan-Song Ma tectonic belt (also known as Ailaoshan paired metamorphic belt), which is ca. 1000 km long and 20–200 km wide, includes the Diancangshan, Ailaoshan and Yaoshan groups. These three groups have been considered parts of the Proterozoic basement of the South China Craton (Fig. 1b). Fourteen least altered diabase and amphibolite samples in the vicinity of the Mili and Yaoshan villages from the Ailaoshan and Yaoshan groups, respectively (Fig. 1b), were collected. For more details of the studied samples, please refer to (Liu et al., 2017a).

3. Analytical results

Analytical methods have been listed in Supplementary texts 1–3. Detailed analytical results of Pb-Li-Mg isotopes are given in the Tables 1 and 2. Previous zircon U—Pb analyses have dated the crystallization ages of the diabase and amphibolite to be 139 Ma and 73–68 Ma, respectively (Liu et al., 2017a). The Mili diabases and Yaoshan amphibolites have typical tholeiite compositions, and are characterized by high Na_2O (Na_2O/K_2O = 10.8–60.2, 1.4–4.4), TiO_2 (1.5–1.9 wt%, 0.7–1.5 wt%) and Nb (7.2–9.7 ppm, 8.0–12.3 ppm) contents, and high $(Nb/Th)_{PM}$ (0.58–0.87, 0.89–1.37), $(Nb/La)_{PM}$ (0.54–0.86, 1.20–1.58), Nb/U (16.2–27.2, 20.5–46.3) ratios. Both suites lack Nb—Ta negative

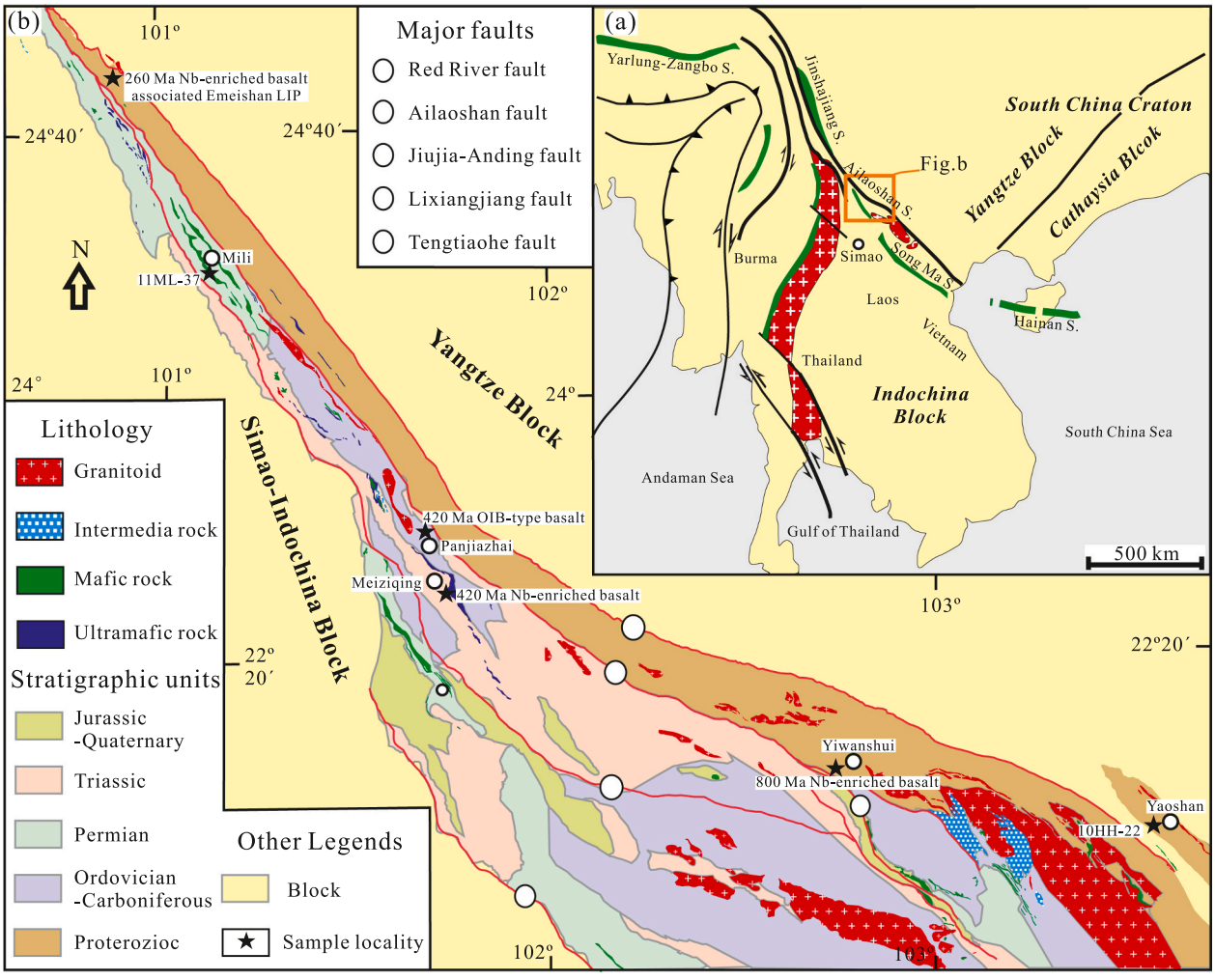

Fig. 1. (a) Tectonic outline of southeast Asia, and (b) geological map of the Ailaoshan area (China). This figure is modified after (Liu et al., 2018).

Table 1
whole-rock Pb isotope analytical results.

Sample	10HH-22 A	10HH-22B	10HH-22C	10HH-22D	10HH-22E	10HH-22 L	11ML-37 A	11ML-37B	11ML-37E	11ML-37Z	11ML-37Z
$^{208}Pb/^{204}Pb$	39.308	39.029	39.056	39.161	39.201	39.112	38.448	38.398	38.416	38.163	38.162
$^{207}Pb/^{204}Pb$	15.663	15.721	15.664	15.661	15.656	15.713	15.557	15.541	15.575	15.528	15.528
$^{206}Pb/^{204}Pb$	18.927	18.609	18.675	18.859	18.873	18.793	18.201	18.152	18.179	18.021	18.020
Pb	3.65	4.18	4.14	2.96	5.68	5.31	4.18	4.18	5.41	4.53	4.53
Th	0.24	0.40	0.20	0.39	0.42	0.27	0.40	0.38	0.40	0.37	0.37
U	0.92	2.20	0.89	0.89	1.20	1.14	2.20	3.68	1.28	1.13	1.13
$(^{208}Pb/^{204}Pb)t$	39.304	39.024	39.054	39.156	39.198	39.110	38.444	38.394	38.412	38.160	38.162
$(^{207}Pb/^{204}Pb)t$	15.661	15.717	15.662	15.660	15.655	15.712	15.554	15.536	15.574	15.527	15.528
$(^{206}Pb/^{204}Pb)t$	18.889	18.530	18.649	18.825	18.848	18.771	18.134	18.033	18.148	17.992	18.020
Δ8/4	84.015	99.416	87.958	76.942	78.428	78.986	89.308	96.541	84.437	78.061	74.862
Δ7/4	12.248	21.778	14.977	12.788	12.095	18.597	9.681	9.014	11.579	8.557	8.358

Table 2
whole-rock Li-Si-Mg isotope analytical results.

Sample	δ^7Li_{LSVEC} ‰	2σ	$\delta^{25}Mg_{DSM-3}$‰	2σ	$\delta^{26}Mg_{DSM-3}$‰	2σ
10HH-22 A	−1.3	0.14	−0.172	0.022	−0.336	0.046
10HH-22 A	−1.27	0.2	−0.174	0.037	−0.34	0.018
10HH-22B	−1.99	0.06	−0.12	0.03	−0.236	0.038
10HH-22C	−1.41	0.1	−0.12	0.016	−0.234	0.06
10HH-22D	−2.39	0.02	−0.138	0.018	−0.265	0.039
10HH-22E	−2.18	0.22	−0.135	0.028	−0.257	0.067
10HH-22 L	−2.19	0.11	−0.148	0.03	−0.293	0.073
11ML-37 A	−2.01	0.17	−0.067	0.024	−0.127	0.049
11ML-37B	−1.43	0.15	−0.065	0.029	−0.115	0.047
11ML-37E	−2.54	0.2	−0.103	0.014	−0.198	0.018
11ML-37Z	−1.77	0.92	−0.075	0.024	−0.143	0.049
11ML-37Z	−1.31	0.15	−0.108	0.057	−0.209	0.081

anomalies on spider diagrams (Fig. 2). These features are akin to typical Nb-enriched basalts (Supplementary Fig. S1b and S1c). Furthermore, 73 Ma OIB-like amphibolites are also identified in the Yaoshan area coexisting with the 68 Ma Yaoshan Nb-enriched amphibolites (Fig. 2). The initial Sr isotopic ratios for the Mili Nb-enriched diabases vary from 0.70509 to 0.70598, and the $\varepsilon_{Nd}(t)$ values range from +1.46 to +3.00. The Yaoshan Nb-enriched amphibolites have $(^{87}Sr/^{86}Sr)i$ ratios of 0.70482–0.70518 and $\varepsilon_{Nd}(t)$ values of +3.59 to +3.81. The Yaoshan OIB-like amphibolite have a $(^{87}Sr/^{86}Sr)i$ ratio of 0.70534 and $\varepsilon_{Nd}(t)$ value of +3.95.

3.1. Pb—Pb isotopes

For Mili diabase samples, $(^{206}Pb/^{204}Pb)i$, $(^{207}Pb/^{204}Pb)i$ and $(^{208}Pb/^{204}Pb)i$ ratios range from 17.99 to 18.15, 15.53–15.57 and 38.16–38.44, respectively, with strongly positive Δ8/4 values (74–97) and slightly positive Δ7/4 values (8.4–11.6) (Figs. 3a and 3b and Table 1). The Yaoshan Nb-enriched amphibolites have strongly positive Δ8/4 values (76.9–88.0) and slightly positive Δ7/4 values (12.1–18.6), with $(^{206}Pb/^{204}Pb)i = 18.65–18.85$, $(^{207}Pb/^{204}Pb)i = 15.66–15.71$ and $(^{208}Pb/^{204}Pb)i = 39.05–39.20$ (Figs. 3a and 3b and Table 1). Pb—Pb isotope analyses have also been carried out on two Yaoshan OIB-like amphibolites, and they show variable Δ8/4 (84.0 and 99.4), Δ7/4 values (12.2 and 21.8), and $(^{206}Pb/^{204}Pb)i$ (18.89 and 18.53), $(^{207}Pb/^{204}Pb)i$ (15.66 and 15.72) and $(^{208}Pb/^{204}Pb)i$ (39.30 and 39.02) ratios. High radiogenic Pb compositions suggest the involvement of a high U/Pb (Th/U) component in their source region. On $(^{206}Pb/^{204}Pb)i$ vs $(^{208}Pb/^{204}Pb)i$ and $(^{207}Pb/^{204}Pb)I$ geochemical diagrams, all samples plot slightly above the North Hemisphere Reference Line(Hart, 1988) and show an affinity to global pelagic sediments (Fig. 3).

3.2. Magnesium isotopes

The Mili diabases have MgO contents of 5.35 to 6.12 wt% and relatively homogeneous $\delta^{26}Mg$ values of −0.115‰ to −0.209‰ (mean

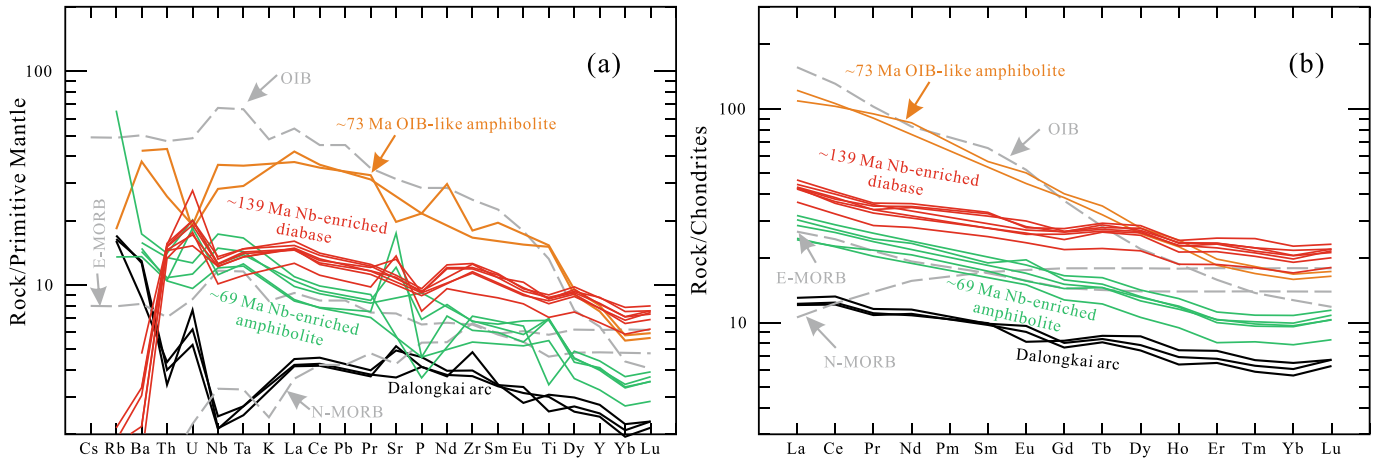

Fig. 2. (a) Primitive mantle-normalized trace element and (b) chondrite-normalized REE patterns spider grams for the OIB-associated Nb-enriched mafic rocks in the Ailaoshan area of the Yunnan-Burma region.

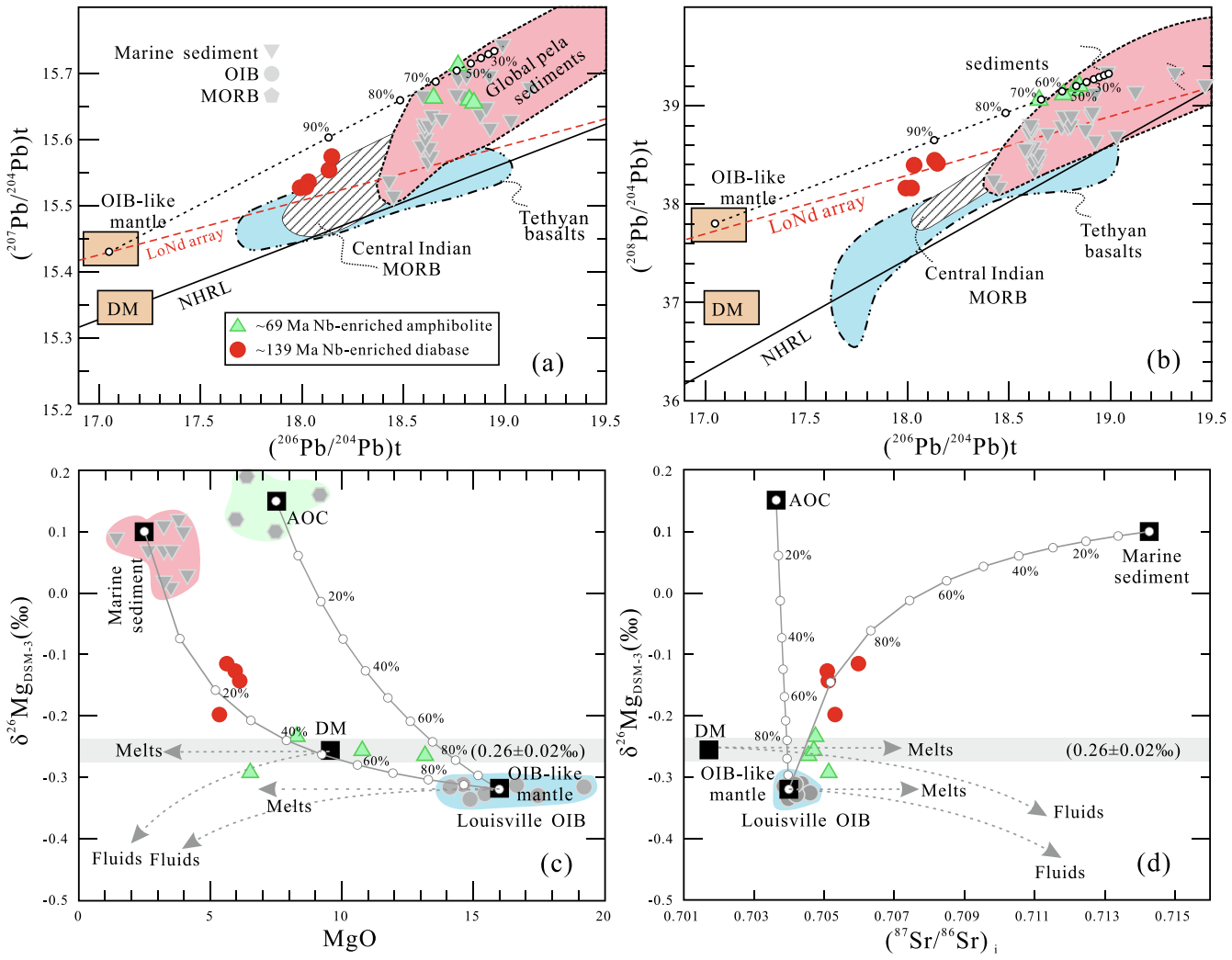

Fig. 3. (a and b) Plots of $^{206}Pb/^{204}Pb$ vs $^{207}Pb/^{204}Pb$ and $^{208}Pb/^{204}Pb$, and (c and d) MgO and $(^{87}Sr/^{86}Sr)_i$ versus $\delta^{26}Mg$ for the HFSE-enriched mafic rocks in the Ailaoshan area. The fields of OIB-like mantle and marine sediments are from refs. (Hart et al., 1986; Hu et al., 2017; Huang et al., 2018; Plank et al., 2007; Weaver, 1991; Zhong et al., 2017). The LoNd array and Northern Hemisphere Reference Line (NHRL) are from ref. (Hart, 1984). The fields of Indian Ocean MORB, Shuanggou and Jinshajiang ophiolites are from refs. (Hamelin and Allègre, 1985; Xu and Castillo, 2004) and references therein. Mixing component OIB-like mantle has $^{206}Pb/^{204}Pb = 17.05$, $^{207}Pb/^{204}Pb = 15.43$, $^{208}Pb/^{204}Pb = 37.80$, Pb = 5.0 ppm, MgO = 16.0 wt%, $\delta^{26}Mg = -0.32‰$, $(^{87}Sr/^{86}Sr)_i = 0.7040$, and Sr = 200.0 ppm. Marine sediments have $^{206}Pb/^{204}Pb = 18.99$, $^{207}Pb/^{204}Pb = 15.74$, $^{208}Pb/^{204}Pb = 39.32$, Pb = 34.0 ppm, MgO = 2.5 wt%, $\delta^{26}Mg = 0.10‰$, $(^{87}Sr/^{86}Sr)_i = 0.71427$, and Sr = 235 ppm. Mixing component AOC has MgO = 7.5 wt%, $\delta^{26}Mg = 0.15‰$, $(^{87}Sr/^{86}Sr)_i = 0.7036$, and Sr = 94.0 ppm.

$= -0.158 \pm 0.05$, $n = 5$) (Fig. 3c and 3d and Table 2). The Nb-enriched amphibolites have MgO contents of 6.52 wt% to 13.17 wt% and relatively homogeneous $\delta^{26}Mg$ values of −0.234‰ to −0.357‰ (mean = -0.287 ± 0.06, $n = 4$). The geographically close OIB-like amphibolites have MgO contents of 6.52 wt% to 6.66 wt% and relatively homogeneous $\delta^{26}Mg$ values of −0.236‰ to −0.340‰ (mean = -0.298 ± 0.03, $n = 3$).

3.3. Lithium isotopes

The Mili diabases have δ^7Li values of −2.54‰ to −1.31‰ (Fig. 4 and Table 2). The Yaoshan Nb-enriched and OIB-like amphibolites have relatively restricted ranges of δ^7Li values, with −2.19 ‰ – -1.41 ‰ and − 1.99 ‰ to −1.27 ‰, respectively. These lithium isotopes are much lighter than those of OIB, fresh MORB, and slab fluids and melts, but heavier than the residual AOC (Fig. 4).

4. Discussion

4.1. Upwelling of OIB-like asthenosphere dominates the HFSEs enrichment

The HFSEs, rare earth elements, Th and U are significantly correlated with immobile Zr (Liu et al., 2017a), indicating their immobile behavior during post-intrusion metamorphism and sub-solidus alteration (Polat and Kerrich, 2002). Crustal contamination was minimal, and fractional crystallization of olivine, clinopyroxene and plagioclase is significant (Liu et al., 2017a). At the same time radiogenic isotopes indicate an heterogeneosu mantle source.

The calc-alkaline to alkaline geochemical variations, median incompatible trace element compositions between OIB and MORB- or arc-like mantle (Fig. 2), weakly depleted Sr—Nd isotopes, and generally positive correlation between Nb and other incompatible trace elements, suggest a binary mixture of OIB and MORB−/arc-like mantle source components (Supplementary Figs. S3 and S4) for the HFSE-enriched magma. The Nb-enriched mafic rocks in the Ailaoshan area coexist with OIB-like rocks, indicating that their source region may contain

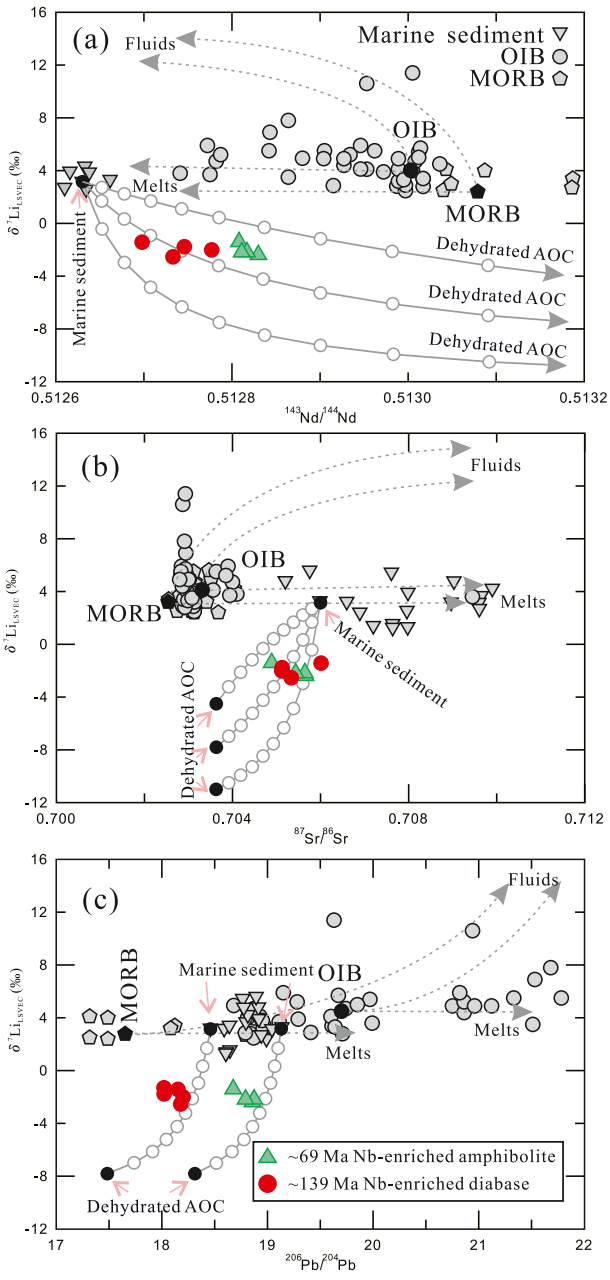

Fig. 4. (a) Diagram of $^{143}Nd/^{144}Nd$ (a), $^{87}Sr/^{86}Sr$ (b) and $^{206}Pb/^{204}Pb$ versus δ^7Li ages for the HFSEs-enriched mafic rocks in the Ailaoshan area. Data for the OIB, marine sediment, MORB and residual AOC are from refs. (Chan et al., 2006; Chan et al., 2009; Leeman et al., 2004; Nishio et al., 2007; Zack et al., 2003), respectively. Mixing component AOC has $^{143}Nd/^{144}Nd = 0.51324$, Nd = 5.34 ppm, $^{87}Sr/^{86}Sr = 0.7036$, Sr = 102 ppm, $^{206}Pb/^{204}Pb = 17.484–18.313$, Pb = 0.26–0.46 ppm, $\delta^7Li = -11‰$, −7.8‰ and − 4.5‰ (Xu and Castillo, 2004; Zack et al., 2003). Marine sediment has $^{143}Nd/^{144}Nd = 0.51263$, Nd = 15.75 ppm, $^{87}Sr/^{86}Sr = 0.7060$, Sr = 124 ppm, $^{206}Pb/^{204}Pb = 18.459–18.130$, Pb = 15.14–13.80 ppm, $\delta^7Li = -3.2‰$ (Chan et al., 2006). Note that $^{143}Nd/^{144}Nd$, $^{87}Sr/^{86}Sr$ and $^{206}Pb/^{204}Pb$ ratios haven't been calculated to the crystallization age.

upwelling OIB-like asthenosphere (Supplementary Fig. S2 and Fig. 2). The presence of OIB-like components in the Ailaoshan area with the Nb-enriched mafic rocks is analogous to the Sulu arc in the southern Philippines and to the Western Mexican arc, where similar Nb-enriched rocks originate from a mantle source mixed with an OIB-like mantle (Petrone and Ferrari, 2008). Metasomatism-free primary OIB-like magma is characterized by extremely high HFSEs contents and alkaline geochemical features, and its mixing with other mantle components could fully explain the HFSE-enriched (Fig. 2), and subalkaline to alkaline elemental compositions in our Nb-enriched rocks (Supplementary Fig. S1a). Thus, involvement of upwelling OIB-like asthenosphere dominates the HFSEs-enriched features of our samples.

4.2. Subducted mélange recycling into OIB-like asthenosphere produces HFSE-enriched arc rocks

The OIB-like mantle is one of the mixing components for the HFSE-enriched mafic rocks, and another component may be MORB (depleted mantle) -like or arc-like mantle. Late Paleozoic Shuanggou ophiolites with typical N-MORB geochemical features in the central Ailaoshan belt could represent the depleted mantle. Radiogenic Sr and Nd isotopes do not fractionate with oceanic crust alteration during slab subduction. The AOC has the same Sr—Nd isotope compositions with the unaltered N-MORB. The peridotites of the Shuanggou ophiolites, taken as representative of N-MORB and also of AOC relatively to their Nd and Sr isotopes compositions (Xu and Castillo, 2004), show high $\varepsilon_{Nd}(t)$ values of +10.3 − +11.5, while $\varepsilon_{Nd}(t)$ value of our OIB-like samples is +3.95. The OIB-like component has similar, but the N-MORB-like component has much more depleted Sr—Nd isotopic compositions than the Mili and Yaoshan Nb-enriched mafic rocks. Besides, the OIB and depleted mantle (DM) show similar Si and Mg isotope compositions, and their mixing cannot explain the low $\delta^{30}Si$ and high $\delta^{26}Mg$ values of our samples (Fig. 3). Mixing between OIB-like and MORB-like mantle components cannot generate Sr-Nd-Mg isotopic compositions of our Nb-enriched rocks.

A possible mixing component may be represented by the arc-like mantle characterized by LILE-enrichment and HFSE-depletion. We calculated trace element mixing models on a number of bivariate diagrams (Supplementary Fig. S4). All the Nb-enriched samples fall along mixing lines between OIB-like and arc-like mantle components, suggesting that their mixing can produce the Nb-enriched geochemical characteristics (Supplementary Fig. S4). Furthermore, their REE compositions can also be explained by OIB-like and arc-like magma mixing (Supplementary Fig. S5). There are two possible origins for the LILE-enriched and HFSE-depleted features of the arc rocks beneath the Yunnan-Burma region: (1) adakitic metasomatism produced by slab melts modify the overlying mantle wedge associated with partial melting of the metasomatized mantle wedge (Rupke et al., 2004); (2) hybrid mélange rocks formed by sediments, AOC and/or hydrated mantle rising as diapirs into the mantle wedge.

For the Mili and Yaoshan Nb-enriched mafic rocks, neither Cretaceous adakites nor evidence for Cretaceous subducting slab melting has been found in the Ailaoshan area, which are a prerequisite for an adakitic metasomatism model. Both adakite and mantle wedge compositions have much heavier Li isotope compositions ($\delta^7Li = +1.8 - +5.1$ and $\delta^7Li = +3.4 \pm 1.4$ ‰, respectively) (Hanna et al., 2020) than our samples.

Marine sediments and AOC can mix to form hybrid mélange rocks along the interface between the subducted slab and the overlying mantle. Mélange subsequently rises as diapirs into the mantle wedge where they dehydrate and melt to form arc magmas (Nielsen and Marschall, 2017). Sediment melts and AOC fluids display similar Sr—Nd isotope compositions but much lower Nd/Sr ratios than their respective bulk counterparts (marine sediment and AOC). Mixing curves of sediment melts and AOC fluids in Sr—Nd isotope space have discernible curvatures from those of mixing between bulk sediment and AOC (Supplementary Fig. S3a)(Nielsen and Marschall, 2017). Our samples plot far away from the mixing lines between sediment melts and AOC fluids, and along those of bulk marine sediment and AOC (Supplementary Fig. S3a). Mixing between the mantle and bulk sediment, and sediment melts follows distinct straight lines (Supplementary Fig. S3b). Our samples show finite Nd isotope and Hf/Nd ratio variation. The Yaoshan HFSEs-enriched rocks plots close to the AOC-sediment mixing

lines, and the Mili rocks fall along horizontal partial melting lines, indicating that their source magma is originated from mixing between AOC and bulk sediment before partial melting.

The role played by subducted mélange is highlighted by Li isotopes. Lithium is a moderately incompatible element in basaltic systems. Its heavy ^{7}Li isotope partitions preferentially into melts and fluids over a residual mantle mineralogy, giving melts and fluids much higher δ^{7}Li values than the residual source rocks (Elliott et al., 2006). Sediment melt and AOC fluid metasomatism will release heavy Li isotopes into the mantle wedge, and modern arc rocks indeed have much higher δ^{7}Li values relative to MORB and OIB (Hanna et al., 2020). The residual marine sediment on the slab interface will have extremely light Li isotope compositions. The AOC often possess extremely light Li isotope compositions with δ^{7}Li values as low as −11‰ (Elliott et al., 2006; Zack et al., 2003). Our Mili rocks show low δ^{7}Li values of −2.54‰ to −1.31‰, and the Yaoshan Nb-enriched rocks have δ^{7}Li values of −2.19 to −1.41 ‰ (Fig. 4). Both are much lower than published values for arc rocks (Hanna et al., 2020), OIB (Nishio et al., 2004) and MORB (Brant et al., 2012; Tomascak et al., 2008). However, addition of residual marine sediment and AOC with low ^{7}Li isotopic compositions (i.e., subducted mélange), rather than sediment melts and AOC fluids, can produce the low δ^{7}Li values in our samples (Fig. 4).

The Yaoshan rocks show similar Pb isotope ratios to the global pelagic sediments (Plank et al., 2007). Both the Mili and Yaoshan rocks have much higher radiogenic Pb compositions, and plot along mixing lines between the OIB-like mantle and global pelagic sediments in Fig. 3. Thus, these Pb compositions also argue for the involvement of marine sediments. The Mili and Yaoshan HFSEs-enriched rocks have heavier δ^{26}Mg values of −0.115‰ to −0.209‰ and − 0.234‰ to −0.357‰ than OIB (Zhong et al., 2017), arc rocks (Teng et al., 2016) and MORB (Liu et al., 2017b). Aqueous Mg^{2+} in subduction zones is enriched in lighter Mg isotope compositions (Wang et al., 2019), and the AOC fluid and sediment melt typically show much lower δ^{26}Mg values (down to −1.3 ‰) than mantle peridotites (Chen et al., 2018). Thus, AOC fluid and sediment melt metasomatism cannot produce the heavy Mg compositions of the Mili and Yaoshan HFSE-enriched rocks (Fig. 3). A component with heavier Mg compositions is required in the source region of our rocks. Sediment melts and AOC fluids release lighter Mg isotope into mantle wedge from the down going slab. Low-temperature alteration of oceanic crust drives the residual AOC and marine sediment to heavier Mg isotopic compositions with weighted average δ^{26}Mg values of 0.00 ± 0.09 ‰ (Huang et al., 2018) and 0.10 ± 0.05 ‰ (e.g., radiolarian-bearing chert) (Hu et al., 2017), respectively (Fig. 3). Mixing of the marine sediments with the OIB can generate the Mg isotope

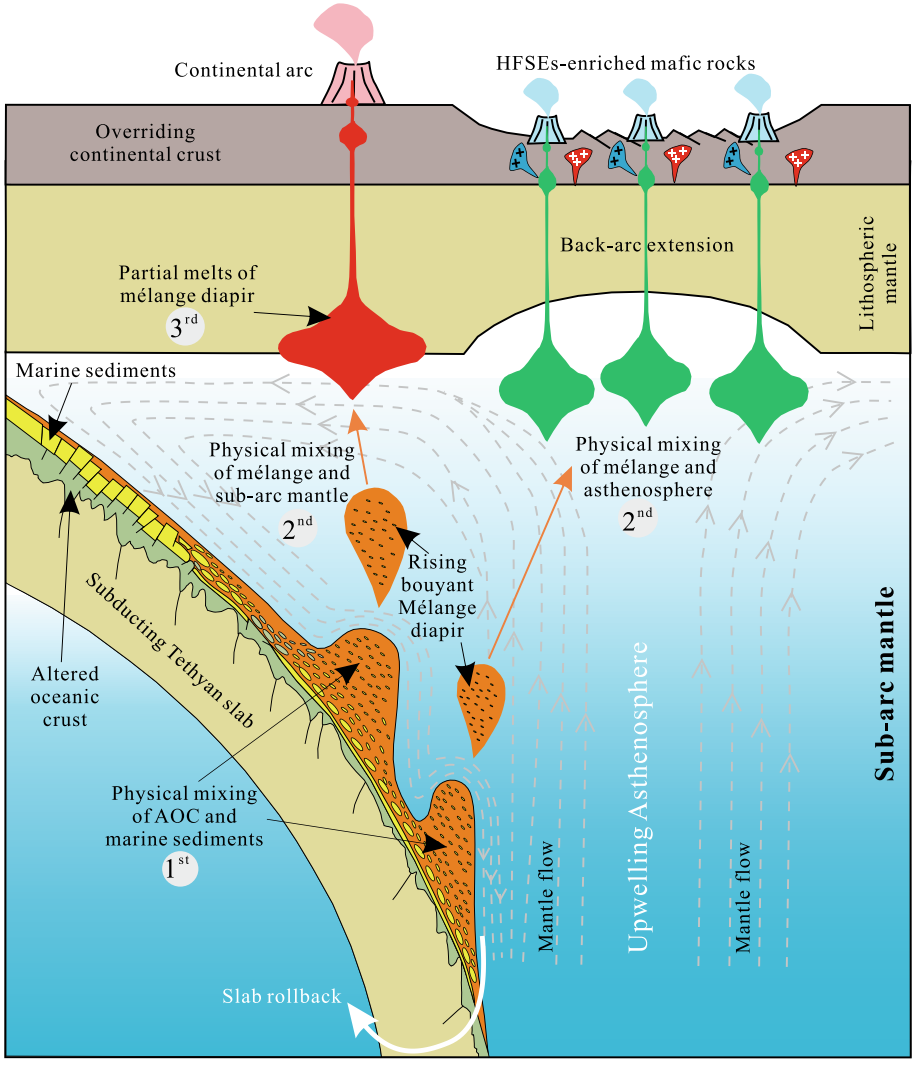

Fig. 5. Schematic cartoon of subducted mélange recycling in upwelling OIB-like asthenosphere depicting two different trajectories for the buoyant mélange diapirs. Mélange diapirs detached from the mantle-slab interface. Some buoyantly upwelled into the mantle wedge, and partially melted at the base of the lithosphere, where diapirs are heated to temperatures >1000–1100 °C after (Nielsen and Marschall, 2017). Others were absorbed into upwelling asthenosphere, and their mixing magma produced the HFSEs-enriched mafic rocks.

compositions of the HFSE-enriched mafic magma.

Consequently, bulk AOC and marine sediment (i.e., subducted mélange) recycling into the upwelling OIB-like asthenosphere produced the HFSE-enriched and Sr-Nd-Pb-Si-Li-Mg isotope characteristics of the HFSE-enriched arc rocks (Fig. 5). The existence of mélange diapirs underneath continental arcs has been evidenced by previous numerical modeling and geophysical observations (Behn et al., 2011; Lin et al., 2021). Subducting marine sediments have lower density than the overlying mantle, and the negative density contrast also causes instabilities along the interface between the subducting slab and the mantle (Behn et al., 2011; Ho, 2019). Thus, the viscosity and density contrasts make the formation and ascent of mélange diapirs possible. When the rising mélange diapirs mix with the mantle wedge, their partial melting will produce HFSE-depleted arc rocks (Fig. 5)(Liu et al., 2022). When the rising mélange diapirs mix with upwelling OIB-like asthenosphere, the generation of the OIB associated HFSE-enriched arc rocks is favored (Fig. 5). The OIB associated HFSE-enriched arc rocks witnessed the subducted mélange recycling and their interactive processes with the upwelling asthenosphere.

Funding

HCL thanks National Key Research and Development Program of China (No. 2021YFA0719000) and CNPC Innovation Found (No. 2021DQ02-0103) for financial support.

Author contributions

HCL and ARH designed the research; HCL provided samples and performed the research and analyzed data; All authors contributed with discussions.

Declaration of Competing Interest

The authors declare that they have no known competing financial interests or personal relationships that could have appeared to influence the work reported in this paper.

Appendix A. Supplementary data

Supplementary data to this article can be found online at https://doi.org/10.1016/j.lithos.2023.107411.

References

Aguillon-Robles, A., Calmus, T., Benoit, M., Bellon, H., Maury, R.O., Cotten, J., Bourgois, J., Michaud, F., 2001. Late miocene adakites and Nb-enriched basalts from Vizcaino Peninsula, Mexico: indicators of East Pacific Rise subduction below Southern Baja California? Geology 29, 531–534.
Azizi, H., Asahara, Y., Tsuboi, M., 2014. Quaternary high-Nb basalts: existence of young oceanic crust under the Sanandaj-Sirjan Zone, NW Iran. Int. Geol. Rev. 56, 167–186.
Behn, M.D., Kelemen, P.B., Hirth, G., Hacker, B.R., Massonne, H.J., 2011. Diapirs as the source of the sediment signature in arc lavas. Nat. Geosci. 4, 641–646.
Brant, C., Coogan, L.A., Gillis, K.M., Seyfried, W.E., Pester, N.J., Spence, J., 2012. Lithium and Li-isotopes in young altered upper oceanic crust from the East Pacific Rise. Geochim. Cosmochim. Acta 96, 272–293.
Castillo, P.R., 2008. Origin of the adakite-high-Nb basalt association and its implications for postsubduction magmatism in Baja California, Mexico. Geol. Soc. Am. Bull. 120, 451–462.
Castillo, P.R., 2012. Adakite petrogenesis. Lithos 134, 304–316.
Castillo, P.R., Solidum, R.U., Punongbayan, R.S., 2002. Origin of high field strength element enrichment in the Sulu Arc, southern Philippines. Geology 30, 707–710.
Castillo, P.R., Rigby, S.J., Solidum, R.U., 2007. Origin of high field strength element enrichment in volcanic arcs: geochemical evidence from the Sulu Arc, southern Philippines. Lithos 97, 271–288.
Chan, L.H., Leeman, W.P., Plank, T., 2006. Lithium isotope composition of marine sediments. Geochem. Geophys. Geosyst. 7, Q06005.
Chan, L.H., Lassiter, J.C., Hauri, E.H., Hart, S.R., Blusztajn, J., 2009. Lithium isotope systematics of lavas from the Cook-Austral Islands: Constraints on the origin of HIMU mantle. Earth Planet. Sci. Lett. 277, 433–442.
Chen, Y., Huang, F., Shi, G.H., Wu, F.Y., Chen, X., Jin, Q.Z., Su, B., Guo, S., Sein, K., Nyunt, T.T., 2018. Magnesium isotope composition of subduction zone fluids as constrained by Jadeitites From Myanmar. J. Geophys. Res.-Solid Earth 123, 7566–7585.
Defant, M.J., Drummond, M.S., 1993. Mount St. Helens: potential example of the partial melting of the subducted lithosphere in a volcanic arc. Geology 21, 541–550.
Deng, J.H., Yang, X.Y., Zhang, L.P., Duan, L.A., Mastoi, A.S., Liu, H., 2020. An overview on the orgin of adakites/adakitic rocks and related porphyry Cu-AU mineralization, Northern Luzon, Philippines. Ore Geol. Rev. 124, 103610.
Elliott, T., Thomas, A., Jeffcoate, A., Niu, Y.L., 2006. Lithium isotope evidence for subduction-enriched mantle in the source of mid-ocean-ridge basalts. Nature 443, 565–568.
Hall, P.S., Kincaid, C., 2001. Diapiric flow at subduction zones: A recipe for rapid transport. Science 292, 2472–2475.
Hamelin, B., Allègre, C.J., 1985. Large scale regional units in the depleted upper mantle revealed by an isotopic study of the southwest India ridge. Nature 315, 196–198.
Hanna, H.D., Liu, X.M., Park, Y.R., Kay, S.M., Rudnick, R.L., 2020. Lithium isotopes may trace subducting slab signatures in Aleutian arc lavas and intrusions. Geochim. Cosmochim. Acta 278, 322–339.
Hart, S.R., 1984. A large-scale isotope anomaly in the Southern Hemisphere mantle. Nature 309, 753–757.
Hart, S.R., 1988. Heterogeneous mantle domains: Signatures, genesis and mixing chronologies. Earth Planet. Sci. Lett. 90 (273), 296.
Hart, S.R., Gerlach, D.C., White, W.M., 1986. A possible new Sr–Nd–Pb mantle array and consequences for mantle mixing. Geochim. Cosmochim. Acta 50, 1551–1557.
Hastie, A.R., Kerr, A.C., Pearce, J.A., Mitchell, S.F., 2007. Classification of altered volcanic island arc rocks using immobile trace elements: development of the Th-Co discrimination diagram. J. Petrol. 48, 2341–2357.
Hastie, A.R., Mitchell, S.F., Kerr, A.C., Minifie, M.J., Millar, I.L., 2011. Geochemistry of rare high-Nb basalt lavas: Are they derived from a mantle wedge metasomatised by slab melts? Geochim. Cosmochim. Acta 75, 5049–5072.
Ho, C.Q., 2019. Conditions of Mélange Diapir Formation, pp. 1–28.
Hu, Y., Teng, F.Z., Plank, T., Huang, K.J., 2017. Magnesium isotopic composition of subducting marine sediments. Chem. Geol. 466, 15–31.
Huang, K.J., Teng, F.Z., Plank, T., Staudigel, H., Hu, Y., Bao, Z.Y., 2018. Magnesium isotopic composition of altered oceanic crust and the global Mg cycle. Geochim. Cosmochim. Acta 238, 357–373.
Kelemen, P.B., Johnson, K.T.M., Kinzler, R.J., Irving, A.J., 1990. High-field-strength element depletions in arc basalts due to mantlemagma interaction. Nature 345, 521–524.
Kepezhinskas, P., Defant, M.J., Drummond, M.S., 1996. Progressive enrichment of island arc mantle by melt-peridotite interaction inferred from Kamchatka xenoliths. Geochim. Cosmochim. Acta 60, 1217–1229.
Kepezhinskas, P., Berdnikov, N., Kepezhinska, N., Konovalova, N., 2022. Adakites, high-Nb basalts and copper-gld depositis in Magamtic arcs and collisional orogens: an overview. Geosciences 12, 29.
Leeman, W.P., Tonarini, S., Chan, L.H., Borg, L.E., 2004. Boron and lithium isotopic variations in a hot subduction zone - the southern Washington Cascades. Chem. Geol. 212, 101–124.
Lin, C.H., Shih, M.H., Lai, Y.C., 2021. Mantle wedge diapirs detected by a dense seismic array in Northern Taiwan. Sci. Rep. 11, 1–12.
Liu, H.C., Wang, Y.J., Cawood, P.A., Guo, X.F., 2017a. Episodic slab rollback and back-arc extension in the Yunnan-Burma region: Insights from Cretaceous Nb-enriched and oceanic-island basalt-like mafic rocks. Geol. Soc. Am. Bull. 129, 698–714.
Liu, H.C., Xia, X.P., Lai, C.K., Gan, C.S., Zhou, Y.Z., Huangfu, P.P., 2018. Break-away of South China from Gondwana: Insights from the Silurian high-Nb basalts and associated magmatic rocks in the Diancangshan-Ailaoshan fold belt (SW China). Lithos 318, 194–208.
Liu, H.C., Neilsen, S.G., Zhu, G.Y., 2022. Sponge-rich sediment recycling in a Paleozoic continental arc driven by mélange melting. Geology 51, 75–79.
Liu, P.P., Teng, F.Z., Dick, H.J.B., Zhou, M.F., Chung, S.L., 2017b. Magnesium isotopic composition of the oceanic mantle and oceanic Mg cycling. Geochim. Cosmochim. Acta 206, 151–165.
Munker, C., Worner, G., Yogodzinski, G., Churikova, T., 2004. Behaviour of high field strength elements in subduction zones: constraints from Kamchatka-Aleutian arc lavas. Earth Planet. Sci. Lett. 224, 275–293.
Nielsen, S.G., Marschall, H.R., 2017. Geochemical evidence for melange melting in global arcs. Sci. Adv. 3, 1–6.
Nishio, Y., Shun'ichi, N., Yamamoto, J., Sumino, H., Matsumoto, T., Prikhod'ko, V.S., Arai, S., 2004. Lithium isotopic systematics of the mantle-derived ultramafic xenoliths: implications for EM1 origin. Earth Planet. Sci. Lett. 217, 245–261.
Nishio, Y., Nakai, S., Ishii, T., Sano, Y., 2007. Isotope systematics of Li, Sr, Nd, and volatiles in Indian Ocean MORBs of the Rodrigues Triple Junction: Constraints on the origin of the DUPAL anomaly. Geochim. Cosmochim. Acta 71, 745–759.
Petrone, C.M., Ferrari, L., 2008. Quaternary adakite - Nb-enriched basalt association in the western Trans-Mexican Volcanic Belt: is there any slab melt evidence? Contrib. Mineral. Petrol. 156, 73–86.
Petrone, C.M., Francalanci, L., Carlson, R.W., Ferrari, L., Conticelli, S., 2003. Unusual coexistence of subduction-related and intraplate-type magmatism: Sr, Nd and Pb isotope and trace element data from the magmatism of the San-Pedro-Ceboruco graben (Nayarit, Mexico). Chem. Geol. 193, 1–24.
Plank, T., Kelley, K.A., Murray, R.W., Stern, L.Q., 2007. Chemical composition of sediments subducting at the Izu-Bonin trench. Geochem. Geophys. Geosyst. 8, 1–16.
Polat, A., Kerrich, R., 2002. Nd-isotope systematics of similar to 2.7 Ga adakites, magnesian andesites, and arc basalts, Superior Province: evidence for shallow crustal recycling at Archean subduction zones. Earth Planet. Sci. Lett. 202, 345–360.

Prouteau, G., Maury, R.C., Sajona, F.G., Cotten, J., Cotten, J.L., 2000. Behavior of Niobium, Tantalum and other high field strength elements in adakites and related lavas from The Philippines. Island Arc 9, 487–498.
Reagan, M.K., Gill, J.B., 1989. Coexisting calcalkaline and high-niobium basalts from Turrialba volcano, Costa Rica: implications for residual titanatcj in arc magma sources. J. Geophys. Res. 94, 4619–4633.
Righter, K., Rosas-Elguera, J., 2001. Alkaline lavas in the volcanic front of the western Mexican Volcanic Belt: Geology and petrology of the Ayutla and Tapalpa volcanic fields. J. Petrol. 42, 2333–2361.
Rupke, L.H., Morgan, J.P., Hort, M., Connolly, J.A.D., 2004. Serpentine and the subduction zone water cycle. Earth Planet. Sci. Lett. 223, 17–34.
Teng, F.Z., Hu, Y., Chauvel, C., 2016. Magnesium isotope geochemistry in arc volcanism. Proc. Natl. Acad. Sci. U. S. A. 113, 7082–7087.
Tomascak, P.B., Langmuir, C.H., le Roux, P.J., Shirey, S.B., 2008. Lithium isotopes in global mid-ocean ridge basalts. Geochim. Cosmochim. Acta 72, 1626–1637.
Verma, S.P., Nelson, S.A., 1989. Isotopic and trace element constraints on the origin and evolution of alkaline and calc-alkaline magmas in the Northwestern Mexican Volcanic Belt. J. Geophys. Res. Solid Earth 94, 4531–4544.
Wang, Q., Wyman, D.A., Xu, J.F., Wan, Y.S., Li, C.F., Zi, F., Jiang, Z.Q., Qiu, H.N., Chu, Z. Y., Zhao, Z.H., Dong, Y.H., 2008. Triassic Nb-enriched basalts, magnesian andesites, and adakites of the Qiangtang terrane (Central Tibet): evidence for metasomatism by slab-derived melts in the mantle wedge. Contrib. Mineral. Petrol. 155, 473–490.
Wang, W.Z., Zhou, C., Liu, Y., Wu, Z.Q., Huang, F., 2019. Equilibrium Mg isotope fractionation among aqueous Mg2+, carbonates, brucite and lizardite: Insights from first-principles molecular dynamics simulations. Geochim. Cosmochim. Acta 250, 117–129.
Weaver, B.L., 1991. The origin of ocean island basalt end-member compositions: trace element and isotopic constraints. Earth Planet. Sci. Lett. 104, 381–397.
Wyman, D.A., Ayer, J.A., Devaney, J.R., 2000. Niobium-enriched basalts from the Wabigoon subprovince, Canada: evidence for adakitic metasomatism above an Archean subduction zone. Earth Planet. Sci. Lett. 179, 21–30.
Xu, J.F., Castillo, P.R., 2004. Geochemical and Nd-Pb isotopic characteristics of the Tethyan asthenosphere: implications for the origin of the Indian Ocean mantle domain. Tectonophysics 393, 9–27.
Zack, T., Tomascak, P.B., Rudnick, R.L., Dalpe, C., McDonough, W.F., 2003. Extremely light Li in orogenic eclogites: the role of isotope fractionation during dehydration in subducted oceanic crust. Earth Planet. Sci. Lett. 208, 279–290.
Zhong, Y., Chen, L.H., Wang, X.J., Zhang, G.L., Xie, L.W., Zeng, G., 2017. Magnesium isotopic variation of oceanic island basalts generated by partial melting and crustal recycling. Earth Planet. Sci. Lett. 463, 127–135.